Nanoscale

PAPER

Cite this: *Nanoscale*, 2017, **9**, 11619

Native defects and substitutional impurities in two-dimensional monolayer InSe

Dan Wang, Xian-Bin Li * and Hong-Bo Sun

Received 12th May 2017,
Accepted 15th July 2017

DOI: 10.1039/c7nr03389c

rsc.li/nanoscale

As a burgeoning two-dimensional (2D) semiconductor, InSe holds unique electronic properties and great promise for novel 2D electronic devices. To advance the development of 2D InSe devices, the exploration of n-type and p-type conductivities of InSe is indispensable. With first-principles calculations, we investigate the properties of native defects and substitutional impurities in monolayer InSe, including formation energies and ionization energies. As the traditional jellium scheme encounters an energy divergence for charged defects in 2D materials, an extrapolation approach is adopted here to obtain convergent energies. We find that In vacancy is a deep acceptor and Se vacancy is an electrically neutral defect. All the studied substitutional dopants at In or Se sites have high ionization energies in the range of 0.41–0.84 eV. However, electrons may transport through the defect-bound band edge states in X_{Se} (X = Cl, Br, and I) as a potential source of n-type conductivity.

Two-dimensional (2D) materials have triggered worldwide interest since the successful isolation of graphene.[1] Due to the quantum confinement effects, 2D materials exhibit novel properties which are remarkably different from their three-dimensional (3D) counterparts.[2–9] They show great potential for advanced technological applications, especially in electronics. They are expected to be the next-generation channel materials for high-performance electronic devices on account of their inherent advantage of an atomic-level thickness.[10,11] Among them, InSe has drawn special attention recently.[12] Bulk InSe possesses a layered structure and InSe nanosheets can be mechanically exfoliated from the bulk structure.[12,13] InSe has a bandgap which means that 2D InSe field effect transistor (FET) devices can be readily switched on and off. Both optical studies and theoretical calculations have shown that its bandgap is tunable and depends on the number of layers.[12–16] More recently, stable field effect devices with atomically thin InSe encapsulated by hexagonal boron nitride under an inert atmosphere have been achieved by Bandurin *et al.*[12] The device exhibits a high carrier mobility of 10^3 cm^2 V^{-1} s^{-1} at room temperature, which is comparable to that of black phosphorus[17] and surpasses that of transition metal dichalcogenides.[18] Also, the device nearly shows no degradation over months, which indicates its excellent environmental stability. In addition, a high on/off ratio of 10^7 and a low subthreshold value of 1 mV dec^{-1} measured from the transfer characteristics of multilayer InSe FETs have also been reported.[19] All these experimental and theoretical studies reveal that the burgeoning InSe is a promising candidate for future high-performance electronics.

To advance the industrialized development of 2D InSe electronic devices, a systematic understanding of the defects or doping properties is indispensable, especially the ability to supply carriers.[20] It determines the doping strategies for the realization of n-channel and p-channel FETs, which are the building blocks for integrated circuits. However, defects in 2D semiconductors have been difficult to model theoretically. The straightforward application of the traditional jellium scheme for 3D materials introduces an energy divergence for charged states in 2D systems.[21,22] Recent theoretical progress in addressing the divergent electrostatic energy in periodic 2D systems has allowed for more accurate calculation of defect ionization energies in these systems.[21,22]

In this letter, we adopt the calculation approach of ref. 21 which has been proposed by Wang, Li, and Zhang *et al.* (WLZ extrapolation method) to systematically evaluate the properties of native defects and substitutional impurities in monolayer InSe and then explore its possible n-type and p-type conductivities. The native defects include In vacancy (V_{In}) and Se vacancy (V_{Se}). The acceptor-type impurities include group-IIB elements (on In sites, Zn_{In}, Cd_{In}, and Hg_{In}) and group-VA elements (on Se sites, As_{Se}, Sb_{Se}, and Bi_{Se}), whereas the donor-type impurities include group-IVA (on In sites, Ge_{In}, Sn_{In}, and Pb_{In}) and group-VIIA elements (on Se sites, Cl_{Se}, Br_{Se}, and I_{Se}). For the native defects, V_{In} behaves as a deep acceptor with an ionization energy (IE) of 0.74 eV whereas V_{Se} is an electrically neutral defect. X_{In} (X = Zn, Cd, and Hg) and X_{Se} (X = As, Sb,

State Key Laboratory on Integrated Optoelectronics, College of Electronic Science and Engineering, Jilin University, Changchun 130012, China.
E-mail: lixianbin@jlu.edu.cn

and Bi) are all deep acceptors with the lowest ionization energy of 0.72 eV of Bi_{Se}. However, X_{Se} (X = Cl, Br, and I) may contribute to the n-type conductivity through the defect-bound band edge state[23] though a high IE of 0.46–0.51 eV. To our knowledge, the present study provides a systematic analysis of convergent ionization energies of various defects in 2D InSe which will benefit the functionalization of nanoelectronic devices.

We perform first-principles calculations based on density-functional theory (DFT),[24,25] as implemented in the Vienna *ab initio* simulation package (VASP) codes.[26,27] Projector augmented-wave basis and generalized gradient approximation (GGA) with the Perdew–Burke–Ernzerhof (PBE) functional are employed.[28] The PAW potentials for In and Se include In ($4d^{10}$, $5s^2$ and $5p^1$) and Se ($4s^2$ and $4p^4$) electrons, respectively. The cutoff energy of the plane wave basis is 400 eV. A 3 × 3 × 1 Monkhorst–Pack mesh grid was used for *k*-point sampling. The effects of spin polarization were included. All atoms are relaxed until the Hellmann–Feynman forces on individual atoms are less than 0.02 eV $Å^{-1}$. Using the jellium approximation, the formation energy of defect *d* with charge *q* is given by:[29,30]

$$\Delta H^{(q,d)} = E^{(q,d)}(\text{host} + \text{defect}) - E(\text{host}) + n_d[\mu_d + \mu_d^{\text{ref}}] + q(\varepsilon_{\text{VBM}} + \varepsilon_F) \quad (1)$$

where $E^{(q,d)}$(host + defect) is the total energy of the supercell containing defect *d* in charge state *q*, and *E*(host) is the total energy of the supercell without any defects. μ_d is the atomic chemical potential of the element referenced to the energy in its stable elemental form (either solid or gas) μ_d^{ref}. n_d is the number of atoms being exchanged during defect formation. ε_F is the Fermi energy measured from the valence band maximum (VBM) denoted as ε_{VBM}. The defect transition level is defined by the Fermi energy at which two different charge states (q' and q) of the same defect *d* have the same formation energy $\Delta H^{(q,d)} = \Delta H^{(q',d)}$. Namely,

$$\varepsilon(q/q') + \varepsilon_{\text{VBM}} = \left[E^{(q,d)}(\text{host} + \text{defect}) - E^{(q',d)}(\text{host} + \text{defect})\right]/(q' - q). \quad (2)$$

The IE, which evaluates the ability of defects to produce free carriers, is defined as $\varepsilon(+1/0)$ with respect to the conduction band minimum (CBM) for the donor, whereas an acceptor IE is defined as $\varepsilon(0/-1)$ with respect to the VBM.

The jellium scheme described above has been widely used in 3D materials, but it encounters an energy divergence for charged states of defects in 2D materials (including the charged formation energy and the resulting IE). To obtain a converged IE, we follow the strategy of ref. 21 (WLZ extrapolation method) wherein the asymptotic expression of IE(S, L_z) with varying cell sizes is given as,

$$\text{IE}(S, L_z) = \text{IE}_0 + \frac{\alpha}{\sqrt{S}} + \frac{\beta L_z}{S} \quad (3)$$

where S is the lateral size, L_z is the vacuum size, β is the constant ($\beta = e^2/24\varepsilon_0$). α is the defect-specific Madelung constant and IE_0 is the converged IE, which both can be obtained by the extrapolation of the expression. Here, the dimension of the supercell is varied from 4 × 4 to 6 × 6 for lateral size with a fixed vacuum size L_z of 50 Å.

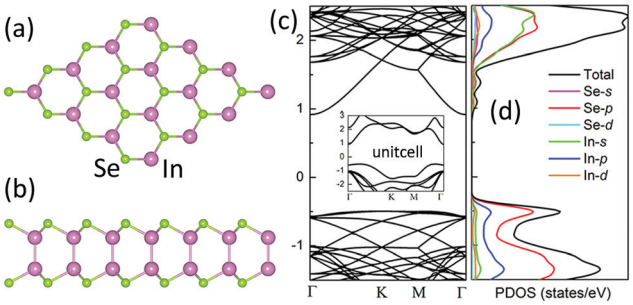

Fig. 1 Top view (a) and side view (b) of the atomic structure of monolayer InSe. Band structure (c) and partial density of states (d) of monolayer InSe with a 4 × 4 supercell. The Fermi level (E_F) is at 0 eV. The inset in (c) shows the band structure of monolayer InSe with a unit cell.

Monolayer InSe is composed of a structure with a sequence of Se–In–In–Se layers, as shown in Fig. 1(a) and (b). The calculated lattice parameter of monolayer InSe is 4.01 Å, which is in agreement with previous theoretical and experimental values.[31,32] Each Se atom forms three bonds with the neighboring In atoms, whereas each In atom forms three bonds with the neighboring Se atoms and one bond with another In atom in the same vertical direction. The two covalently bonded In atoms can be regarded as a whole, denoted as (In_2). Then, InSe can be regarded as (In_2)Se_2. For (In_2)Se_2, each (In_2) has six nearest neighboring Se atoms and each Se has three nearest neighboring (In_2) wholes. Since each (In_2) has 6 valence electrons and 2 of them constitute the covalent bond of In–In, each (In_2) donates 4 electrons to six neighboring Se atoms. Each Se accepts 2 electrons from three neighboring (In_2). Thus, the net charge transfer within any formula unit of (In_2)Se_2 is zero, *i.e.* 4 − 2 × 2 = 0. This means that the electron balance is fulfilled according to the electron counting model (ECM).[33] As such, 2D InSe has a gap. The calculated band structure and partial density of states of monolayer InSe with a 4 × 4 supercell are shown in Fig. 1(c) and (d). It has an indirect bandgap of 1.42 eV with the CBM being at the Γ point and the VBM located between K and M points. The VBM is mainly derived from the p orbits of In and Se while the CBM is mainly derived from the s orbits of In and the p orbits of Se atoms. We also show the band structure of monolayer InSe with a unit cell in the inset of Fig. 1(c), wherein the band gap is also 1.42 eV and the VBM is located between Γ and K.

The calculated atomic and electronic structures of the native defects (V_{In} and V_{Se}) in monolayer InSe are shown in Fig. 2. For V_{In}, three spin-up defect states denoted as 1, 2, and 5, and three spin-down defect states marked as 3, 4, and 6 are generated within the band gap, see Fig. 2(a). Since states 1 and 2 are mostly degenerate and their charge density distributions are similar, only state 1 is displayed in real space. For the same reasons, the charge density distributions of state 3 (similar

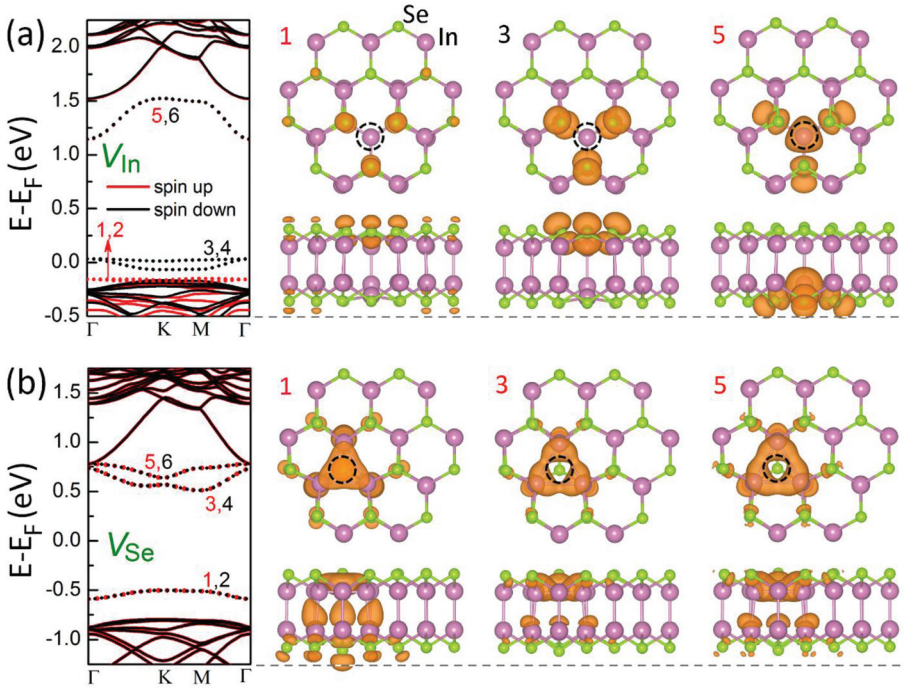

Fig. 2 (a) The spin-polarized band structures of V_{In} and the charge density distributions of the defect states marked as 1, 3, and 5 in the band structure. (b) The spin-polarized band structures of V_{Se} and the charge density distributions of the defect states marked as 1, 3, and 5 in the band structure (as in both cases, states 2, 4, and 6 exhibit similar characteristics with 1, 3, and 5, respectively, so their charge density distributions are not shown here). Red/black lines and numbers for spin up/down. The isosurface is $0.001e/\alpha_0^{-3}$, where α_0 is the Bohr radius. The Fermi level (E_F) is at 0 eV. Dashed circles denote the positions of the defects.

to 4) and state 5 (similar to 6) are displayed in real space. States 1 and 2 mainly come from the p orbits of three neighboring Se atoms. These states have a certain degree of overlap with the VBM and thus exhibit an extensive electronic distribution like that of a band edge. States 3 and 4 also originate from the p orbits of three neighboring Se atoms while states 5 and 6 are mainly contributed by the s orbits of the In atom (originally bonded to the removed In atom) and the p orbits of its adjacent Se atoms. The partially occupied states 3 and 4 are closer to the VBM than the CBM, which means a greater possibility to accept an electron as an acceptor. For V_{Se}, there are three defect states for each spin, see Fig. 2(b). States 1 and 2 mainly come from the p orbits of the surrounding In and Se atoms, whereas states 3–6 are mostly contributed by the s and p orbits of the neighboring In atoms around V_{Se}, and the p orbits of the surrounding Se atoms. As the occupied states 1 and 2 are far from the CBM and the unoccupied states 3–6 are far from the VBM, it is very difficult for V_{Se} to donate or accept an electron.

To explore the possible n-type and p-type conductivities of InSe, which are required for 2D electronic devices, the doping properties of extrinsic impurities, including group-IIB elements (on In sites, Zn_{In}, Cd_{In}, and Hg_{In}), group-IVA (on In sites, Ge_{In}, Sn_{In}, and Pb_{In}), group-VA elements (on Se sites, As_{Se}, Sb_{Se}, and Bi_{Se}), and group-VIIA elements (on Se sites, Cl_{Se}, Br_{Se}, and I_{Se}) have been investigated. The calculated band structures of these defects are shown in Fig. 3. For the X_{In} defect (X = Zn, Cd, Hg, Ge, Sn, and Pb), there is a spin-up state marked as 1 and a spin-down state marked as 2 within the band gap, see Fig. 3(a)–(f). States 1 and 2 are occupied by one electron in total. This means that they can accept another electron to be fully occupied in total, or donate the electron to be fully unoccupied in total. These states are close to the VBM for X_{In} (X = Zn, Cd, and Hg) and then are prone to accept an electron, whereas the states are close to the CBM for X_{In} (X = Ge, Sn, and Pb) and then are prone to donate an electron. Therefore, X_{In} (X = Zn, Cd, and Hg) are acceptors and X_{In} (X = Ge, Sn, and Pb) are donors. Considering Zn_{In} and Ge_{In} as representatives, we show the real-space charge density distributions of state 2 (similar to 1) of Zn_{In} and state 1 (similar to 2) of Ge_{In}, see Fig. 4(a) and (b). It can be seen that these states mainly originate from the orbits of X, X-bonded In, and their adjacent six Se atoms, which just constitute one formula unit of $(InX)Se_2$ like $(In_2)Se_2$ discussed above. According to the ECM analyses, when an In atom is replaced with an X element (here, considering X = Zn and Ge for illustration), the In–In pair in the unit of $(In_2)Se_2$ changes to an In–X pair. As Zn/Ge has one electron less/more than In, there is a lack/excess of one electron in the unit of $(InX)Se_2$ (X = Zn/Ge) compared to that of $(In_2)Se_2$. As such, the unit of $(InZn)Se_2$ acts as an acceptor and the unit of $(InGe)Se_2$ acts as a donor.

The calculated band structures of the X_{Se} defect (X = As, Sb, Bi, Cl, Br, and I) are shown in Fig. 3(g)–(l). For X_{Se} (X = As, Sb, and Bi), one spin-up state labeled as 1 and one spin-down

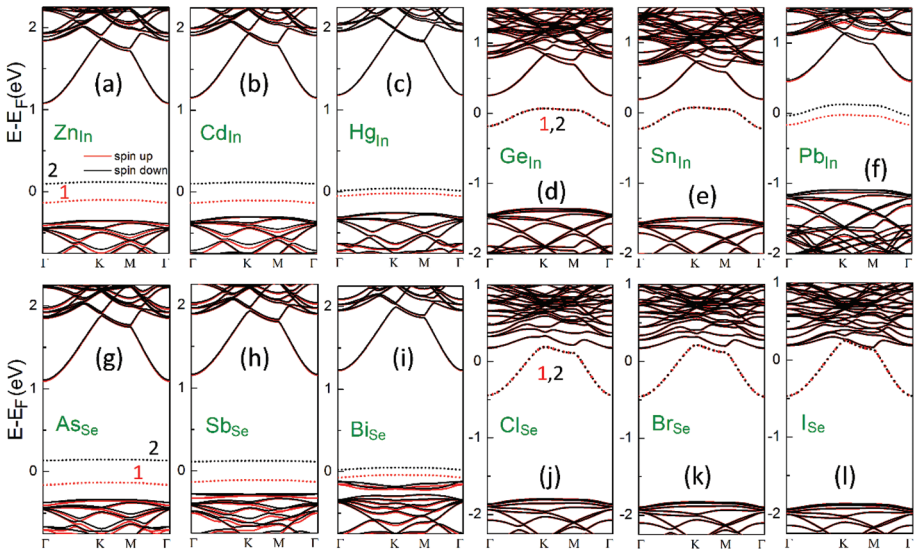

Fig. 3 The spin-polarized band structures of X_{In} (X = Zn, Cd, and Hg), X_{In} (X = Ge, Sn, and Pb), X_{Se} (X = As, Sb, and Bi), and X_{Se} (X = Cl, Br, and I). Red/black lines and numbers for spin up/down. The Fermi level (E_F) is at 0 eV.

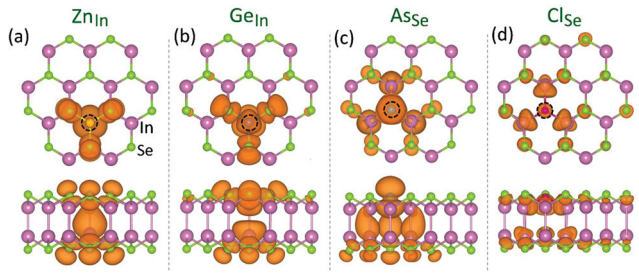

Fig. 4 The charge density distributions of the defect states of Zn_{In}, Ge_{In}, As_{Se}, and Cl_{Se} (marked as 2 for acceptors Zn_{In} and As_{Se}, 1 for donors Ge_{In} and Cl_{Se} in Fig. 3). The isosurface is $0.0005e/\alpha_0{}^3$, where α_0 is the Bohr radius. Dashed circles denote the positions of the defects.

state labeled as 2 are found to be generated and are close to the VBM. These two states possess one electron in total and tend to accept another one from the VBM. Thus, X_{Se} (X = As, Sb, and Bi) are acceptors. In contrast, for X_{Se} (X = Cl, Br, and I), the inclusion of X (X = Cl, Br, and I) into InSe caused little change in the band structures. The excess electrons of X (X = Cl, Br, and I) than those of Se occupy the CBM spontaneously, see states 1 and 2 in Fig. 3(j)–(l). This means that X_{Se} (X = Cl, Br, and I) are shallow donors. Considering As_{Se} and Cl_{Se} as representatives, the real-space charge density distributions of state 2 (similar to 1) of As_{Se} and state 1 (similar to 2) of Cl_{Se} are shown in Fig. 4(c) and (d). These states are mainly contributed by the orbits of X, the Se directly under X, and three adjacent In–In pairs. The distribution of the state in Cl_{Se} exhibits a more delocalized character because of the mixing feature with the CBM of the state. The occupied CBM in X_{Se} (X = Cl, Br, and I) is denoted as the defect-bound band edge state in the following discussions.

The above discussion according to the ground-sate electronic structure of defects is qualitative. To quantitatively evaluate the stability and the ability to supply carriers of the defects, the converged formation energies in the neutral (0) and charged states (+1 for donors, −1 for acceptors) are calculated according to the method of ref. 21 (WLZ extrapolation method), as shown in Fig. 5. For the neutral state, the formation energies are presented for both the In- and Se-rich conditions. It can be clearly seen that V_{In} and X_{In} (X = Zn, Cd, Hg, Ge, Sn, and Pb) have lower formation energies under the Se-rich conditions, whereas V_{Se} and X_{Se} (X = As, Sb, Bi, Cl, Br, and I) have lower formation energies under the In-rich conditions. This can be understood that under the Se-rich conditions the low concentration of the In element facilitates the formation of In vacancy (V_{In}) and In-substituted doping (X_{In}), and *vice versa* under the In-rich conditions. For V_{In} and V_{Se}, charge states of (+1) and (−1) are both considered in each case. The stable states of V_{In} are found to be (0) and (−1) when the Fermi level is inside the band gap. The (0/−1) transition level of V_{In} is located at 0.74 eV above the VBM, which means a deep acceptor. The (+1/0) transition level of V_{In} is located at 0.16 eV below the VBM, which means that V_{In} can hardly donate an electron as a donor. For V_{Se}, the only stable state is found to be (0) when the Fermi level is within the band gap [here, the (+1/0) transition level is 0.08 eV below the VBM while the (0/−1) transition level is 0.45 eV above the CBM]. Thus, V_{Se} is an electrically neutral defect in the monolayer InSe and cannot provide electrons or holes for the system. The formation of V_{Se} is relatively easier (with neutral formation energies of 1.10 eV) than V_{In} (with neutral formation energies of 1.91 eV) under their respective preferred conditions.

For the cases of substitutional acceptors, the neutral formation energies of X_{In} (X = Zn, Cd, and Hg) (−0.33 eV, −0.21 eV, and 0.30 eV under the preferred Se-rich conditions, respectively) are lower than that of X_{Se} (X = As, Sb, and Bi)

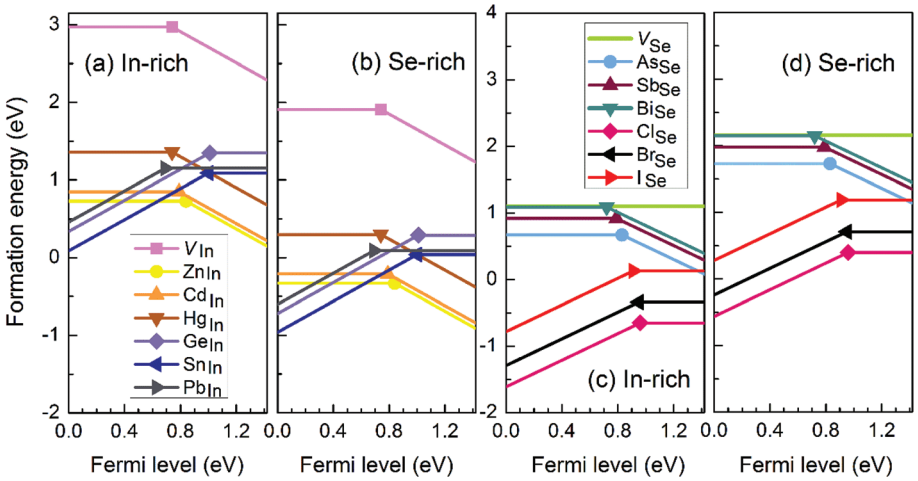

Fig. 5 The converged formation energies as a function of the Fermi level for the native and substitutional defects. (a) and (b) show the V_{In} and In-substituted defects in monolayer InSe. (c) and (d) show the V_{Se} and Se-substituted defects in monolayer InSe. Formation energies of defects are shown for [(a) and (c)] In-rich conditions and [(b) and (d)] Se-rich conditions. The Fermi level varies from 0 at the VBM to 1.42 eV at the CBM according to the calculated PBE band gap of monolayer InSe.

(0.67 eV, 0.92 eV, and 1.09 eV under the preferred In-rich conditions, respectively). In contrast, the transition levels of X_{In} (X = Zn, Cd, and Hg) (0.84 eV, 0.79 eV, and 0.74 eV above the VBM) are comparable to that of X_{Se} (X = As, Sb, and Bi) (0.83 eV, 0.79 eV, and 0.72 eV above the VBM), see Fig. 5. These results hint that X_{In} (X = Zn, Cd, and Hg) and X_{Se} (X = As, Sb, and Bi) are all deep acceptors. For the case of substitutional donors, X_{Se} (X = Cl, Br, and I) (formation energies: −0.65 eV, −0.34 eV, and 0.13 eV under the preferred In-rich conditions, respectively) and X_{In} (X = Ge, Sn, and Pb) (formation energies: 0.29 eV, 0.04 eV, and 0.09 eV under the preferred Se-rich conditions, respectively) are all easy to form. The transition levels of X_{In} (X = Ge, Sn, and Pb) are 0.41 eV, 0.42 eV, and 0.73 eV below the CBM, respectively. Notably, though X_{Se} (X = Cl, Br, and I) show shallow donor states in the band structures shown in Fig. 3(j)–(l), their IEs are 0.46 eV, 0.47 eV, and 0.51 eV below the CBM, respectively, which indicates that they are deep donors. This discrepancy can be understood with the unique ionization picture of defects in 2D materials.[23] In 2D materials, when the carrier is ionized to band edges, it is still bound to the charged defect due to the weak screening. This means that the IE contains two parts, one (IE_1) is the energy required to excite the carrier to the corresponding band edge, and the other one (IE_2) is the energy required to free the carrier from the bound defects. For X_{Se} (X = Cl, Br and I), the excess electron occupies the CBM spontaneously after doping, see states 1 and 2 in Fig. 3(j)–(l), which means that $IE_1 = 0$ and $IE = IE_2$. Moreover, with a reasonable defect density, state 1 can form a band and the wave functions tend to overlap, which will facilitate electron transport. In addition, the overlap can be further enhanced by increasing the screening such as adding a substrate or gate voltage.

Since the GGA method with the PBE functional underestimates band gaps, which will affect the determination of defect level positions, care should be taken to identify how the defect level shifts with an opening band gap. In this work, we carry out hybrid functional calculations (Heyd–Scuseria–Ernzerhof, HSE[34]) for several typical cases including the acceptor Hg_{Zn} and the donors Cl_{Se} and I_{Se}. Also, eqn (3) is applied to obtain the size-independent ionization energies. In the HSE calculations, 45% non-local Hatree Fock exchange and the gamma point are included. The HSE band gap of monolayer InSe is 2.91 eV, which is well consistent with the previous GW result (2.95 eV).[35] For the acceptor Hg_{Zn}, the PBE ionization energy is 0.74 eV and the HSE further deepens the acceptor level with an ionization energy of 1.29 eV. In contrast, the ionization energies of Cl_{Se} and I_{Se} become even shallower in the HSE calculations, being 0.37 eV and 0.45 eV compared to the PBE results (0.46 eV for Cl_{Se} and 0.51 eV for I_{Se}). This is ascribed to (and completely reflect) the conduction band edge characteristic of the states [states 1 and 2 in Fig. 3(j)–(l)] occupied by the excess electron of the X element in X_{Se} (X = Cl, Br, and I). These results further prove that X_{Se} (X = Cl, Br, and I) should be good candidates for n-type doping.

In summary, we systematically investigated the properties of native defects and substitutional impurities in monolayer InSe with first-principles calculations. For charged states of these defects, the converged energies are obtained with the approach proposed in ref. 21 (WLZ extrapolation method). It is found that V_{In} is a deep acceptor and V_{Se} is an electrically neutral defect which cannot offer electrons or holes. All the substitutional defects including X_{In} (X = Zn, Cd, Hg, Ge, Sn, and Pb), X_{Se} (X = As, Sb, Bi, Cl, Br, and I) have high ionization energies in the range of 0.41 eV–0.84 eV. However, for X_{Se} (X = Cl, Br, and I), the electrons may transport through the defect band which is mixed with the CBM. Therefore, X_{Se} (X = Cl, Br and I) can be regarded as promising candidates for n-type conductivity of monolayer InSe.

Acknowledgements

The work was supported by the 973 Program (No. 2014CB921303), and the National Natural Science Foundation of China (No. 11374119, 91423102 and 61307119). Also, we acknowledge the High-Performance Computing Center (HPCC) at Jilin University for calculation resources.

References

1 K. S. Novoselov, A. K. Geim, S. V. Morozov, D. Jiang, Y. Zhang, S. V. Dubonos, I. V. Grigorieva and A. A. Firsov, *Science*, 2004, **306**, 666–669.
2 B. Radisavljevic, A. Radenovic, J. Brivio, V. Giacometti and A. Kis, *Nat. Nanotechnol.*, 2011, **6**, 147–150.
3 L. Li, Y. Yu, G. J. Ye, Q. Ge, X. Ou, H. Wu, D. Feng, X. H. Chen and Y. Zhang, *Nat. Nanotechnol.*, 2014, **9**, 372–377.
4 K. F. Mak and J. Shan, *Nat. Photonics*, 2016, **10**, 216–226.
5 Z. Shi and C. V. Singh, *Nanoscale*, 2017, **9**, 7055–7062.
6 J. Xiao, Z. Ye, Y. Wang, H. Zhu, Y. Wang and X. Zhang, *Light: Sci. Appl.*, 2015, **4**, e366.
7 J. Yang, R. Xu, J. Pei, Y. W. Myint, F. Wang, Z. Wang, S. Zhang, Z. Yu and Y. Lu, *Light: Sci. Appl.*, 2015, **4**, e312.
8 Y. Abate, S. Gamage, Z. Li, V. Babicheva, M. H. Javani, H. Wang, S. B. Cronin and M. I. Stockman, *Light: Sci. Appl.*, 2016, **5**, e16162.
9 W. Strek, B. Cichy, L. Radosinski, P. Gluchowski, L. Marciniak, M. Lukaszewicz and D. Hreniak, *Light: Sci. Appl.*, 2015, **4**, e237.
10 M. Chhowalla, D. Jena and H. Zhang, *Nat. Rev. Mater.*, 2016, **1**, 16052.
11 Y. Yoon, K. Ganapathi and S. Salahuddin, *Nano Lett.*, 2011, **11**, 3768–3773.
12 D. A. Bandurin, A. V. Tyurnina, G. L. Yu, A. Mishchenko, V. Zolyomi, S. V. Morozov, R. K. Kumar, R. V. Gorbachev, Z. R. Kudrynskyi, S. Pezzini, Z. D. Kovalyuk, U. Zeitler, K. S. Novoselov, A. Patane, L. Eaves, I. V. Grigorieva, V. I. Fal'ko, A. K. Geim and Y. Cao, *Nat. Nanotechnol.*, 2017, **12**, 223–227.
13 G. W. Mudd, S. A. Svatek, T. Ren, A. Patane, O. Makarovsky, L. Eaves, P. H. Beton, Z. D. Kovalyuk, G. V. Lashkarev, Z. R. Kudrynskyi and A. I. Dmitriev, *Adv. Mater.*, 2013, **25**, 5714–5718.
14 S. Lei, L. Ge, S. Najmaei, A. George, R. Kappera, J. Lou, M. Chhowalla, H. Yamaguchi, G. Gupta, R. Vajtai, A. D. Mohite and P. M. Ajayan, *ACS Nano*, 2014, **8**, 1263.
15 M. Brotons-Gisbert, D. Andres-Penares, J. Suh, F. Hidalgo, R. Abargues, P. J. Rodriguez-Canto, A. Segura, A. Cros, G. Tobias, E. Canadell, P. Ordejon, J. Wu, J. P. Martinez-Pastor and J. F. Sanchez-Royo, *Nano Lett.*, 2016, **16**, 3221–3229.
16 G. W. Mudd, M. R. Molas, X. Chen, V. Zolyomi, K. Nogajewski, Z. R. Kudrynskyi, Z. D. Kovalyuk, G. Yusa, O. Makarovsky, L. Eaves, M. Potemski, V. I. Fal'ko and A. Patane, *Sci. Rep.*, 2016, **6**, 39619.
17 L. Li, F. Yang, G. J. Ye, Z. Zhang, Z. Zhu, W. Lou, X. Zhou, L. Li, K. Watanabe, T. Taniguchi, K. Chang, Y. Wang, X. H. Chen and Y. Zhang, *Nat. Nanotechnol.*, 2016, **11**, 593–597.
18 X. Cui, G. H. Lee, Y. D. Kim, G. Arefe, P. Y. Huang, C. H. Lee, D. A. Chenet, X. Zhang, L. Wang, F. Ye, F. Pizzocchero, B. S. Jessen, K. Watanabe, T. Taniguchi, D. A. Muller, T. Low, P. Kim and J. Hone, *Nat. Nanotechnol.*, 2015, **10**, 534–540.
19 S. Sucharitakul, N. J. Goble, U. R. Kumar, R. Sankar, Z. A. Bogorad, F. C. Chou, Y. T. Chen and X. P. Gao, *Nano Lett.*, 2015, **15**, 3815–3819.
20 S. B. Zhang, *J. Phys.: Condens. Matter*, 2002, **14**, R881–R903.
21 D. Wang, D. Han, X.-B. Li, S.-Y. Xie, N.-K. Chen, W. Q. Tian, D. West, H.-B. Sun and S. B. Zhang, *Phys. Rev. Lett.*, 2015, **114**, 196801.
22 H.-P. Komsa and A. Pasquarello, *Phys. Rev. Lett.*, 2013, **110**, 095505.
23 D. Wang, D. Han, X.-B. Li, N.-K. Chen, S.-Y. Xie, D. West, W. Q. Tian, V. Meunier, H.-B. Sun and S. Zhang, Low-Energy Excitation to Defect-Bound Band Edge States in Two-Dimensional Semiconductors and its Effect on Carrier Transport (under review), 2017.
24 P. Hohenberg and W. Kohn, *Phys. Rev.*, 1964, **136**, B864–B871.
25 W. Kohn and L. J. Sham, *Phys. Rev.*, 1965, **140**, A1133–A1138.
26 G. Kresse and J. Furthmiiller, *Phys. Rev. B: Condens. Matter*, 1996, **54**, 11169–11186.
27 G. Kresse and J. Furthmiiller, *Comput. Mater. Sci.*, 1996, **6**, 15–50.
28 J. P. Perdew, K. Burke and M. Ernzerhof, *Phys. Rev. Lett.*, 1996, **77**, 3865–3868.
29 S. B. Zhang and J. E. Northrup, *Phys. Rev. Lett.*, 1991, **67**, 2339–2342.
30 D. Han, D. West, X.-B. Li, S.-Y. Xie, H.-B. Sun and S. B. Zhang, *Phys. Rev. B: Condens. Matter*, 2010, **82**, 155132.
31 C. Sun, H. Xiang, B. Xu, Y. Xia, J. Yin and Z. Liu, *Appl. Phys. Express*, 2016, **9**, 035203.
32 S. A. Semiletov, *Kristallografiya*, 1958, **3**, 288–292.
33 M. C. Lucking, J. Bang, H. Terrones, Y.-Y. Sun and S. Zhang, *Chem. Mater.*, 2015, **27**, 3326–3331.
34 J. Heyd, G. E. Scuseria and M. Ernzerhof, *J. Chem. Phys.*, 2003, **118**, 8207–8215.
35 L. Debbichi, O. Eriksson and S. Lebegue, *J. Phys. Chem. Lett.*, 2015, **6**, 3098–3103.

